

Application of LADRC Based on the IMFO Algorithm for Multi-Area Interconnected AGC Problems

Gonggui Chen, Yifan Chen, Yi Xiang, Ping Zhou, Xianjun Zeng and Hongyu Long

Abstract—This paper proposes an improved novel bionic intelligent Moth-Flame Optimization (MFO) algorithm optimized linear active disturbance rejection control (LADRC) strategy for automatic generation control (AGC) problems. LADRC is a control strategy that combines linear extended state observer (LESO) and traditional proportional-derivative (PD) control, with the advantages of its resistance to disturbance and simplicity. The three-order LADRC controller is designed in load frequency control (LFC) system. The Improved MFO (IMFO) algorithm is proposed by Cauchy mutation strategy and self-adaptive weight to overcome the weaknesses in easily falling into local optima and poor optimization search accuracy, and the IMFO algorithm is employed for tuning the parameters of LADRC. Besides, an objective function takes account of the performance index integral-time-multiplied-AE (ITAE) with dynamic indicators, which is used to improve the effectiveness of LADRC. The proposed control strategy is tested for robustness in a two-area non-reheat thermal system and compared with recent control methods published in the literature. As a result, its superiority is demonstrated for the lowest cost function values of ITAE = 0.0036, ITSE = 1.24E-05, ISE = 6.81E-05 and IAE = 0.0086. To further explore the potential of the LADRC controller based on the IMFO algorithm, it is also extended to a two-area nonlinear system and an unequal three-area reheat system. The performance indicator functions and dynamic performance indicators are analyzed qualitatively in the meantime.

Index Terms—Automatic Generation Control, LADRC, IMFO, Governor Dead Band

Manuscript received October 8, 2021; revised March 6, 2022. This work was supported by the National Natural Science Foundation of China under Grant 51207064.

Gonggui Chen is a professor of Key Laboratory of Industrial Internet of Things and Networked Control, Ministry of Education, Chongqing University of Posts and Telecommunications, Chongqing 400065, China; (e-mail: chenggp@126.com).

Yifan Chen is a graduate student of Chongqing University of Posts and Telecommunications, Chongqing 400065, China (e-mail: 17855378192@163.com).

Yi Xiang is a senior engineer of the Northwest Branch of State Grid Corporation of China, Xi'an 710048, China (e-mail: xiangy@nw.sgcc.com.cn).

Ping Zhou is a senior engineer of Economic and Technology Research Institute, State Grid Chongqing Electric Power Company, Chongqing 401120, China (e-mail: 153326062@qq.com).

Xianjun Zeng is a senior engineer of State Grid Chongqing Electric Power Company, Chongqing 400015, China (e-mail: 13594255525@139.com).

Hongyu Long* is a professor level senior engineer of Chongqing Key Laboratory of Complex Systems and Bionic Control, Chongqing University of Posts and Telecommunications, Chongqing 400065, China (corresponding author to provide phone: +8613996108500; e-mail: longhongyu20@163.com).

I. INTRODUCTION

DUE to the growth of the economy and progress of society, the electric network continues to make expansion and promotes its complexity. Frequency is an integral indicator used for measuring power system stability and security, which must be adjusted to the nominal value in standard running conditions. Automatic generation control (AGC) has obtained frequent application in the secondary control loop for load frequency control (LFC) [1], and it realizes the feedback control on load fluctuations through regulating generator output power. Under the real multi-area power system, area control error (ACE) comprises frequency variance and tie-line power exchange. If the system is subject to load disturbance, ACE will be determined as 0 via AGC. Modern power systems have proposed increasingly higher demand for LFC, reflected by the pursuit for a quicker regulation rate and superior dynamic performance.

Recently, many researchers have surveyed AGC and put forward plenty of countermeasures [1, 2]. At the beginning, classical Proportional-Integral (PI) controllers and Proportional-Integral-Derivative (PID) controllers were employed by LFC [3] because of their precise structure, low cost, as well as prominent dynamic response. With the growing complexity in modern power systems, conventional PI controllers gradually expose some drawbacks in performance, including long transient time, multiple overshoots and large transient frequency deviation [4]. For improving LFC precision and robustness, a few advanced control methods, such as Optimal Control Methods [5], Adaptive Control Methods [6, 7], Variable Structure and Sliding Mode Control Methods [8, 9], Predictive Control Methods [10], and Intelligent Control Methods [11, 12] have been adopted for solving LFC problems. Meantime, numerous intelligent optimization algorithms are applied in optimizing controller effect, for instance, PSO [11], GA [13], DE [14], BFOA [15, 16] and GWO [17]. The prominent dynamic response based on aforementioned advanced control methods brings competitiveness. In the meantime, the system turns into complex and the design of controllers depends upon the model in the controlled system. Therefore, there are difficulties in designs against the real industrial environment. Developing a control strategy having anti-disturbance, robustness performance and simple design that does not completely depend upon the controlled object model is awfully imperative.

Active disturbance rejection control (ADRC) technology of Professor Hanjingqing [18] has gained more applications

in the LFC field in recent years. According to reference [19], big probability variation's genetic algorithm was used for optimizing the ADRC controller. Reference [20] developed a LFC strategy of pumped storage units by using linear active disturbance rejection technology (LADRC). In view of reference [21], Q-learning algorithm can be taken for selecting adaptive parameters for ADRC in multi-area interconnected power system. In reference [22], it is primarily utilized in the research on nonlinear problems. More studies are required to deepen the use of LADRC in LFC. The Moth-Flame Optimization (MFO) algorithm is a new bionic algorithm that has been manifested to have the advantages of robustness, structural simplicity and effectiveness in practice, and has also been adopted for the optimization of controller parameters in LFC problems recently [23]. In above, the improved MFO (IMFO) algorithm optimized LADRC control strategy is proposed in this paper, which attempts to apply the LADRC to the AGC problems and searches the parameters of controllers by the IMFO algorithm through the modified objective function. The main contributions as: (1) Application and design of a new controller LADRC for the AGC problems solutions, and the IMFO algorithm is raised by introducing the Cauchy mutation and adaptive weight strategies to tune the parameters of LADRC controllers; (2) To enhance the dynamic performance of the responses of the system frequency deviation and tie-line deviation, a modified objective function combining integral-time-multiplied-AE (ITAE), overshoot, settling time and appropriate weights is acquired based on the control characteristics of the LADRC; (3) The proposed control strategy is analyzed comprehensively in the two-area non-reheat thermal system; (4) To validate the potential of the proposed control strategy, extending it to two-area non-linear system and unequal three-area reheat thermal power system; (5) To demonstrate the advantages of the proposed control strategy in each of

the power systems, the results are compared with the recent proposed control methods, involving DE, hBFOA-PSO, CRAZY_PSO, MFO based PI, GWO, MFO based PID, hPSO-PS based Fuzzy PI (FPI), and IACO based Fuzzy PID (FPID).

In the following sections, the studied system and the control strategy are introduced in section II, the improvement of the MFO algorithm is described in section III, the simulation results are presented in section IV in detail, and finally this article is concluded in section V.

II. POWER SYSTEM MODEL

A. LFC Model

The dynamic model of the two-area interconnected non-reheat power system is introduced in this section, which is widely used in LFC research. As is shown in Fig.1, each control area contains three inputs and two outputs. The inputs include the controller output u , load disturbance ΔP_L and tie-line power error ΔP_{tie} . The outputs are the generator frequency Δf and ACE. In multi-area interconnected power systems, tie-line power deviation and frequency deviation are considered at the same time. ACE is defined as:

$$ACE = B\Delta f + \Delta P_{tie} \quad (1)$$

Each area consists of LADRC controller, turbine, generator, load and governor. In the process of analyzing and designing the control system, the transfer function is established in the model.

From [24], the Governor is represented by the transfer function:

$$G_g(s) = \frac{\Delta P_v(s)}{\Delta P_g(s)} = \frac{1}{1 + T_g s} \quad (2)$$

The transfer function of a turbine is given as [24]:

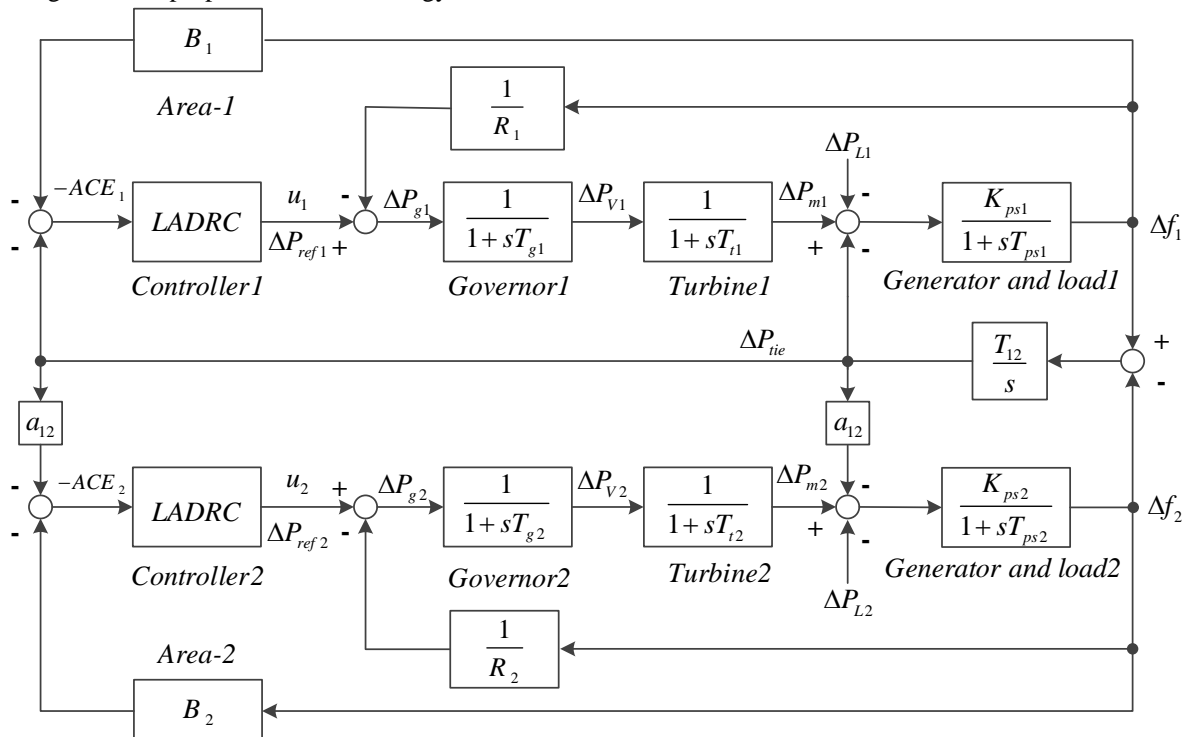


Fig.1. Transfer function model of two-area power system

$$G_r(s) = \frac{\Delta P_m(s)}{\Delta P_v(s)} = \frac{1}{1+T_r s} \quad (3)$$

The generator and load are represented by the transfer function [24]:

$$G_{GL}(s) = \frac{K_{ps1}}{1+sT_{ps1}} \quad (4)$$

In Fig.1, B_1 and B_2 are the frequency bias parameters; ACE_1 and ACE_2 are area control errors; u_1 and u_2 are the outputs from LADRC controller; R_1 and R_2 are the governor speed regulation parameters in p.u. Hz; T_{g1} and T_{g2} are the speed governor time constants in seconds; T_{t1} and T_{t2} are the turbine time constants in seconds; ΔP_{V1} and ΔP_{V2} are the governor output command (p.u.); ΔP_{m1} and ΔP_{m2} are the change in turbine output powers; ΔP_{L1} and ΔP_{L2} are the load demand changes; K_{ps1} and K_{ps2} are the gains of generator and load; T_{ps1} and T_{ps2} are the time constant of generator and load in seconds; T_{12} is the synchronizing coefficient; ΔP_{tie} is the incremental change in tie line power (p.u.); Δf_1 and Δf_2 are the system frequency deviations in Hz. a_{12} is a coefficient. Nominal values of system parameters are illustrated in Appendix A.

B. Controller Structure

LADRC is comprised of three main components, which are linear extended state observer (LESO), linear feedback control law, disturbance compensation. For interconnected power systems with complex structure and severe coupling, LADRC technology takes various uncertainties of the controlled object model as disturbances. Then the disturbances will be estimated and compensated through LESO to eliminate external disturbances quickly and reduce impacts from coupling. The LADRC, which is upgraded on a conventional PID controller, offers superior dynamic performance [25]. Additionally, the design of a LADRC is only required to know the input, output and relative order of the controlled model, and is not dependent on the exact model of the studied system. Based on the structural characteristics of the LFC system, this paper is configured with a three-order LADRC controller in each area, and the structure is given in Fig.2. Three-order LADRC allows the closed-loop dominant apices of the LFC system to be in the negative half-plane, ensuring system stability. As is clarified in Fig.2, u is the disturbance compensation control law, respectively. K_1 , K_2 and K_3 are linear error feedback rates. b is the gain of the model and r is the reference input.

The core idea of the three-order LADRC is to estimate the disturbances of the system via LESO, and then use linear feedback control law to calm the system at the equilibrium point. Linear feedback control law combines linear state feedback errors and derivatives of each order of the errors.

For a three-order controlled object, LESO can be designed as:

$$\begin{cases} \dot{z}_1 = z_2 + l_1(y - z_1) \\ \dot{z}_2 = z_3 + l_2(y - z_1) \\ \dot{z}_3 = z_4 + l_3(y - z_1) + bu \\ \dot{z}_4 = l_4(y - z_1) \end{cases} \quad (5)$$

Define $L_0 = [l_1, l_2, l_3, l_4]^T$ as the observer gain vector. z_1, z_2 and z_3 are the estimated values of the state variable, and z_4 is the total disturbance of the system. The disturbance compensation link is described as below:

$$u(t) = \frac{-z_4(t) + u_0(t)}{b} \quad (6)$$

To simplify the process of parameter tuning, two variables are introduced in the literature [26]: the controller bandwidth w_o and the observer bandwidth w_c .

While we choose $l_1 = 4*w_o$, $l_2 = 6*w_o^2$, $l_3 = 4*w_o^3$, $l_4 = w_o^4$, all observer poles are placed at $-w_o$, i.e.:

$$s^4 + l_1 s^3 + l_2 s^2 + l_3 s + l_4 = (s + w_o)^4 \quad (7)$$

Meanwhile, if we choose $K_1 = w_c^3$, $K_2 = 3*w_c^2$, $K_3 = 3*w_c$, all closed loop poles of the linear error feedback controller are configured at $-w_c$, i.e.:

$$s^3 + K_1 s^2 + K_2 s + K_3 = (s + w_c)^3 \quad (8)$$

It is evident that only three variables need to be considered in the control structure of LADRC namely: b , w_o and w_c . Among them, b is the adaptive parameter, and the value of b is related to the structure of the studied system. The value of w_o is positively related to the observation speed of the linear observer, and it also causes the observer to be more sensitive to noise. Moreover, the size of w_c is positively related to the response speed of the system and negatively related to stability. It is significant to select the appropriate values of controller parameters to find the optimal controller effect. On the basis of literature [26], the relationship of w_o equals to five times w_c is effective on improving the control performance, which makes w_c and b the only parameters to be tuned.

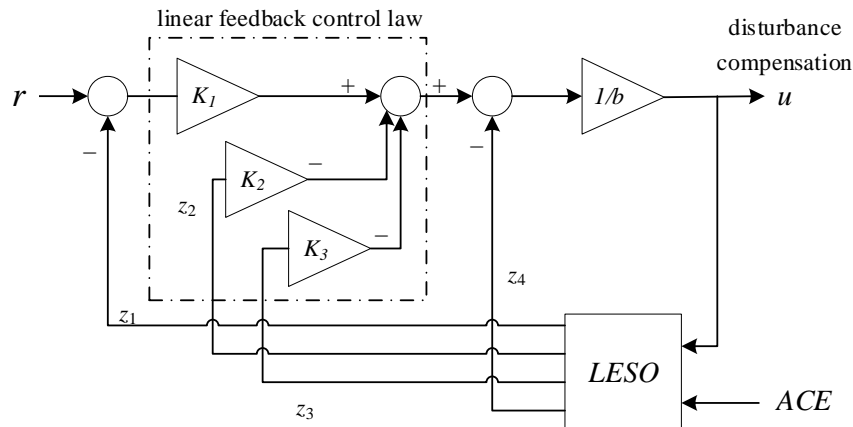


Fig.2. Three-order LADRC structure diagram

C. Optimization Problem

At this stage, the core work of this paper is to ensure the lowest frequency deviation (Δf) and tie-line power deviation (ΔP_{tie}) response during the power system is subjected to load disturbances. In research of LFC, four performance indicator functions are widely used in the parameter optimization of controllers [27]: ITAE, ITSE (integral-time-multiplied-SE), and ISE (integral-squared error), and IAE (integral-absolute error). For the power system shown in Fig.1, the expressions for performance indexes in time domain are given in (9)-(12). In the following equations, t_{sim} is the range of simulation time.

$$J_1 = ITAE = \int_0^{t_{sim}} (|\Delta f_1| + |\Delta f_2| + |\Delta P_{tie}|) \cdot t \cdot dt \quad (9)$$

$$J_2 = ITSE = \int_0^{t_{sim}} (|\Delta f_1|^2 + |\Delta f_2|^2 + |\Delta P_{tie}|^2) \cdot t \cdot dt \quad (10)$$

$$J_3 = ISE = \int_0^{t_{sim}} (|\Delta f_1|^2 + |\Delta f_2|^2 + |\Delta P_{tie}|^2) \cdot dt \quad (11)$$

$$J_4 = IAE = \int_0^{t_{sim}} (|\Delta f_1| + |\Delta f_2| + |\Delta P_{tie}|) \cdot dt \quad (12)$$

When a load disturbance occurs in the system suddenly, gentle frequency fluctuations can be achieved by shorter settling time and overshoot. Therefore, at the moment of optimizing the controller effect, the requirements of both settling time and overshoot are considered as small as possible. Hence, both settling time and overshoot are given a thought to the design process of performance indicators. The feedback compensation of the LADRC control is extremely fast, which is reflected in the small settling time but bringing in a degree of oscillations to the power system. To assure the proportion of overshoot and settling time, suitable weights are confirmed to balance their relationship after several simulation experiments. In this paper, the objective function in (13) is utilized:

$$J_5 = ITAE + w_1 * (|OS| + |US|) + w_2 * T_s \quad (13)$$

where w_1 and w_2 are the weighting factors, in order to make each part reflect its respective advantages in the process of optimization. The weighting factors are chosen as $w_1 = 0.5$ and $w_2 = 0.0008$. And OS is the sum of peak overshoot of Δf_1 , Δf_2 , and ΔP_{tie} . US is the sum of peak undershoot of Δf_1 , Δf_2 , and ΔP_{tie} . T_s is the sum of settling time of Δf_1 , Δf_2 , and ΔP_{tie} .

From above, the optimization problem for the controller is transformed into constrained optimization problem, where the constraint is the range of parameters of the controller. The lower limit of the objective function is found within the constraint range.

Minimize $J_i (i=1,2,3,4,5)$ subjected to:

$$\begin{cases} w_{c \min} \leq w_c \leq w_{c \max} \\ b_{\min} \leq b \leq b_{\max} \\ w_o = 5 * w_c \end{cases} \quad (14)$$

In the above formulas, max and min are the top and bottom limitations of the respective LADRC controller parameters. The minimum values of w_c and b are chosen as 0, the maximum values of w_c and b are chosen as 10 and 200. w_c and b are found as the optimal individuals in the IMFO algorithm, which is described in the next section.

III. IMPROVED MOTH-FLAME OPTIMIZATION ALGORITHM (IMFO)

A. Standard MFO Algorithm

The MFO algorithm is a novel intelligent optimization algorithm proposed by Seyedali Mirjalili in 2015, inspired by a special navigation mechanism of moths at night: transverse orientation [28]. The process of a moth spiraling around a light source is abstracted as an optimal process, where the position of the moth is the optimal solution of the problem to be solved, and the moth flight space is the solution space of the problem. There are two populations with a one-to-one correspondence involved in the process of finding the optimal solution as candidate solutions: the moth and the flame. The differences between these two populations lie in the iterative patterns and the fitness functions they bring in, with the moth seeking solutions in the solution space while the flame is the optimal solution for successive generations of moths.

Initially, the moth population M and the flame population F are both represented as matrices of n rows and d columns in equation (15). n as the number of the population and d as the number of dimensions, whose corresponding matrices of fitness values OM and OF are given in (16).

$$M = \begin{bmatrix} m_{1,1} & m_{1,2} & \dots & m_{1,d} \\ m_{2,1} & m_{2,2} & \dots & m_{2,d} \\ \vdots & \vdots & \ddots & \vdots \\ m_{n,1} & m_{n,2} & \dots & m_{n,d} \end{bmatrix} \quad (15)$$

$$F = \begin{bmatrix} F_{1,1} & F_{1,2} & \dots & F_{1,d} \\ F_{2,1} & F_{2,2} & \dots & F_{2,d} \\ \vdots & \vdots & \ddots & \vdots \\ F_{n,1} & F_{n,2} & \dots & F_{n,d} \end{bmatrix}$$

$$OM = \begin{bmatrix} OM_1 \\ OM_2 \\ \dots \\ OM_n \end{bmatrix}, \quad OF = \begin{bmatrix} OF_1 \\ OF_2 \\ \dots \\ OF_n \end{bmatrix} \quad (16)$$

During the iteration, each moth is updated around the position of its respective flame in the manner of (17):

$$S(M_i, F_j) = D_i \cdot e^{bl} \cdot \cos(2\pi l) + F_j \quad (17)$$

where M_i is the i -th moth and F_j is the j -th flame, D_i is the absolute distance between M_i and F_j defined as (18), b is a constant for defining the shape of the logarithmic spiral, and l is a random number in $[-1,1]$.

$$D_i = |F_j - M_i| \quad (18)$$

The number of flames is updated in an adaptive way:

$$flame_no = round\left(n - t \times \frac{n-1}{itmax}\right) \quad (19)$$

The $flame_no$ is the number of flames in the current generation. t is the number of current iterations and $itmax$ is the total number of iterations.

Throughout the whole algorithm process, the moth continuously searches for individuals in the feasible domain, and the obtained individual positions are brought into the fitness function to return the fitness value. The local optimum searched by the moth in each flight is saved as the position of the flame, and the number of flames is gradually decreased to 1, thus ensuring an efficient global optimum solution.

B. Improved MFO Algorithm for LFC

The MFO algorithm has significant shortcomings in being easy to encounter with local optimum and poor search precision. To solve this problem, two improvement strategies are proposed in this paper: Cauchy mutation strategy and adaptive weight, which will be described in detail as follows.

Cauchy distribution is characterized by a relatively small peak at the origin and a longer distribution at both ends. This feature can produce greater perturbation in the vicinity of the current mutant individual [29]. The standard Cauchy distribution function in (20) is used to jump out the local extremes in this paper, and use the update formula (21) for the position of flames.

$$f(x) = \frac{1}{\pi(1+x^2)} \quad (20)$$

$$x_{best_flame} = x_{best_flame} + x_{best_flame} * Cauchy(0,1) \quad (21)$$

During the moth population moves to the next position, the adaptive weight defined in (22) is introduced and the improved formula is as (23). The introduced adaptive weights could reduce the influence of individual moths in successive generations and facilitate the depth search around the current optimal solution.

$$w = \sin\left(\frac{\pi * t}{2 * itmax} + \pi\right) + 1 \quad (22)$$

$$M_i = |F_j - M_i| \cdot e^{bl} \cdot \cos(2\pi l) + \omega \cdot F_j \quad (23)$$

The IMFO algorithm adopts Cauchy mutation strategy to update the flame position to enhance the randomness of flight tracks of moths and the scope of search space, so as to improve the global search capability of the algorithm. In the process of moth population update, smaller adaptive weights are used to improve the search accuracy of local optimum. Thereby, IMFO is proposed to optimize LADRC. During the optimization of the LADRC parameters by the IMFO algorithm, (w_c, b) determine the position of the individual moths and the fitness value is obtained through the objective function J_i . In a word, the ultimate goal is to search for the optimal parameters (w_c, b) and obtain the minimum fitness value. The flowchart is given in Fig.3.

IV. RESULTS AND DISCUSSIONS

In this paper, the study of the system is completed in the Matlab/Simulink environment. The IMFO algorithm is programmed in the .m file for the optimization of the controller parameters, whose fitness values are obtained from the objective function written in the .m file. The controller parameter values from the IMFO algorithm are input into the system model in a separate file to be simulated. Besides, based on the experience of existing studies, some

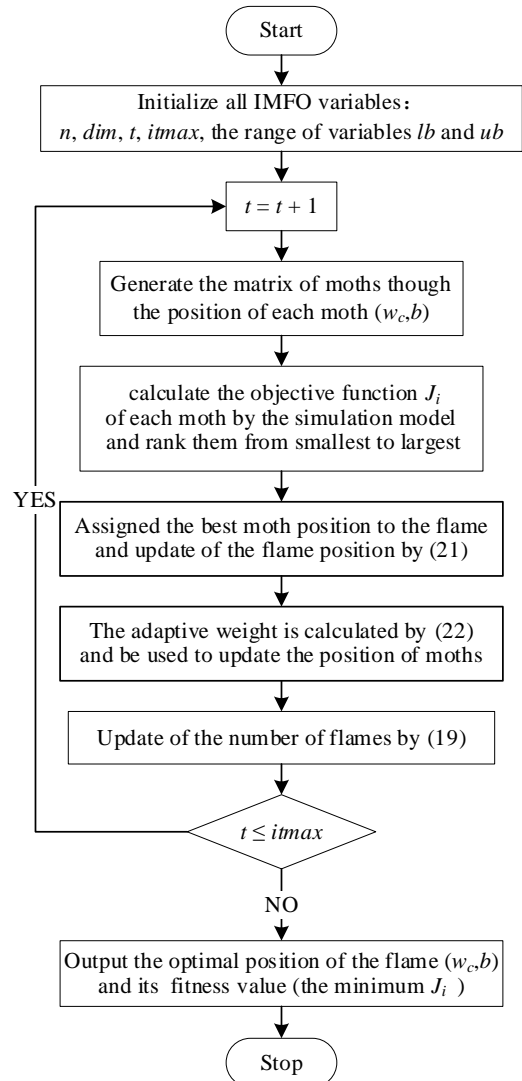


Fig. 3. The flowchart of IMFO algorithm for LFC

parameters in the IMFO algorithm are specified to ensure the efficiency of the optimization search. The size of double populations is defined as 30, the maximum number of iterations is 100, $b = 1$ and $t = [-1, 1]$. Simulations were performed in the MATLAB R2019a environment on an Intel, Core i5-7500 computer with 3.40 GHz and 16 GB of RAM. The values of the LADRC parameters are selected among optimizations of 20 times, and the various experimental results under the studied system are analyzed in the following.

A. Two-area non-reheat thermal system

The two-area non-reheat thermal system is widely used in LFC studies, so the optimization method proposed in this article is mainly tested in this system, which is shown in Fig.1. The relevant parameters are indicated in Appendix. A. 10% step load perturbation (SLP) is given in area-1 at $t = 0$ s. First, to prove the superiority of the IMFO optimized LADRC control strategy proposed, the standard MFO algorithm optimized PID controller and the standard MFO algorithm optimized LADRC controller are adopted to compare. The performance indicator ITAE is used in the optimization process to maintain the consistency of the objective function, and the controller parameters with different control strategies are given in TABLE I, and the response curves of the system power deviation and tie-line

TABLE I
OPTIMIZED VALUES OF PID/LADRC BASED ON MFO/IMFO

Algorithm	Controller parameters					
MFO PID	K_{p1}	K_{i1}	K_{d1}	K_{p2}	K_{i2}	K_{d2}
	1.0729	1.9999	0.3864	1.9999	0.0008	0.5097
LADRC MFO	w_{c1}	w_{o1}	b_1	w_{c2}	w_{o2}	b_2
	10	50	142.6119	2.0022	10.0113	87.5701
LADRC IMFO	10	50	95.4852	1.9321	9.6607	143.9482

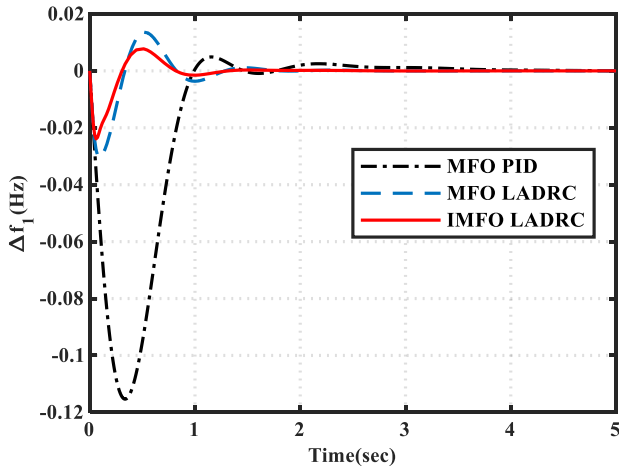


Fig. 4. Change in f_1 due to 10% disturbance in area 1

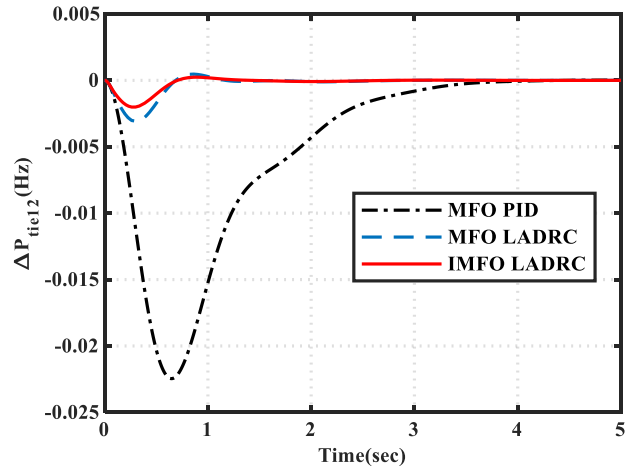


Fig. 6. Change in P_{tie} due to 10% disturbance in area

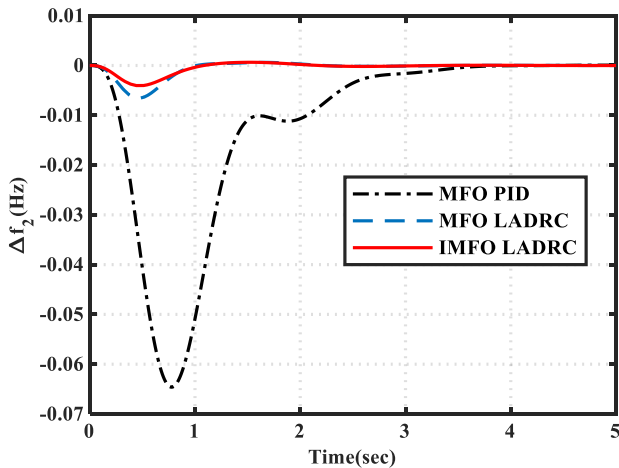


Fig. 5. Change in f_2 due to 10% disturbance in area 1

power deviation (Δf_1 , Δf_2 , ΔP_{tie}) are shown in Fig.4-6. As can be seen from the figures: i) compared with the traditional PID controller, the three-order LADRC can provide fast feedback compensation speed with significant regulation effect when the system is subject to external

disturbances; ii) the LADRC controller optimized by the IMFO algorithm can obtain a better dynamic performance, which is reflected in smaller settling time and calmer overshoot phenomenon.

Furthermore, the objective function J_5 is designed to overcome the oscillation problem of LADRC. To verify it, four common performance indicators ITAE, ITSE, ISE, IAE are used to compare with J_5 . The controller parameters tuned with the various objective functions and the corresponding objective function values are given in TABLE II. The response curves for Δf_1 , Δf_2 and ΔP_{tie} are shown in Fig.7-9. In comparison to the other four objective functions, J_5 gets the smallest fitness values of ITAE (0.0056), ITSE (1.24E-05), ISE (6.81E-05), and IAE (0.0086). Simultaneously, since J_5 takes settling time and overshoot into consideration, the response curves in Fig.7-9 show that the controller optimized by J_5 allows the system to reach the nominal value more quickly and smoothly as the disturbance occurs. Accordingly, LADRC tuning based on the IMFO algorithm is turned out to be effective in improving control performance.

TABLE II
RESULTS OF IMFO ALGORITHM UNDER DIFFERENT OBJECTIVE FUNCTIONS

Algorithm	w_{c1}	w_{o1}	b_1	w_{c1}	w_{o2}	b_2	ITAE	ITSE	ISE	IAE	J_5
J_1 IMFO	10	50	95.4852	1.9321	9.6607	143.9482	0.0056	1.90E-05	9.03E-05	0.0108	0.0277
J_2 IMFO	10	50	123.9605	4.1936	20.9678	63.03957	0.0055	3.36E-05	1.5E-04	0.0134	0.0319
J_3 IMFO	10	50	100.1705	6.4314	32.1572	186.5241	0.0051	2.03E-05	9.92E-05	0.0111	0.0287
J_4 IMFO	10	50	108.3021	6.6849	33.4245	200	0.0059	2.51E-05	1.17E-04	0.0123	0.0311
J_5 IMFO	10	50	83.9030	4.0674	20.3372	96.6481	0.0036	1.24E-05	6.81E-05	0.0086	0.0229

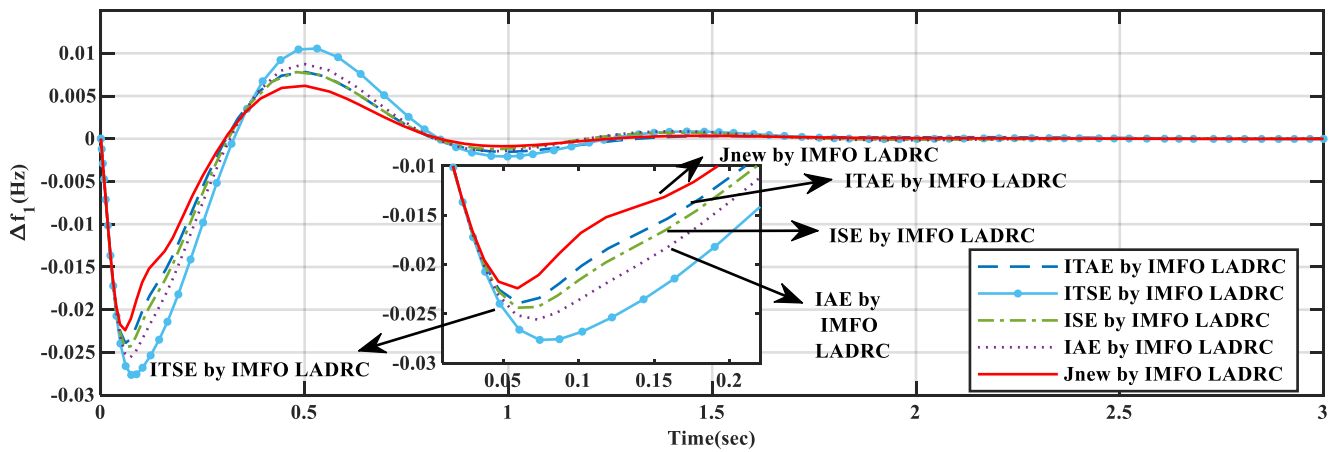


Fig.7. Change in f_1 under different objective

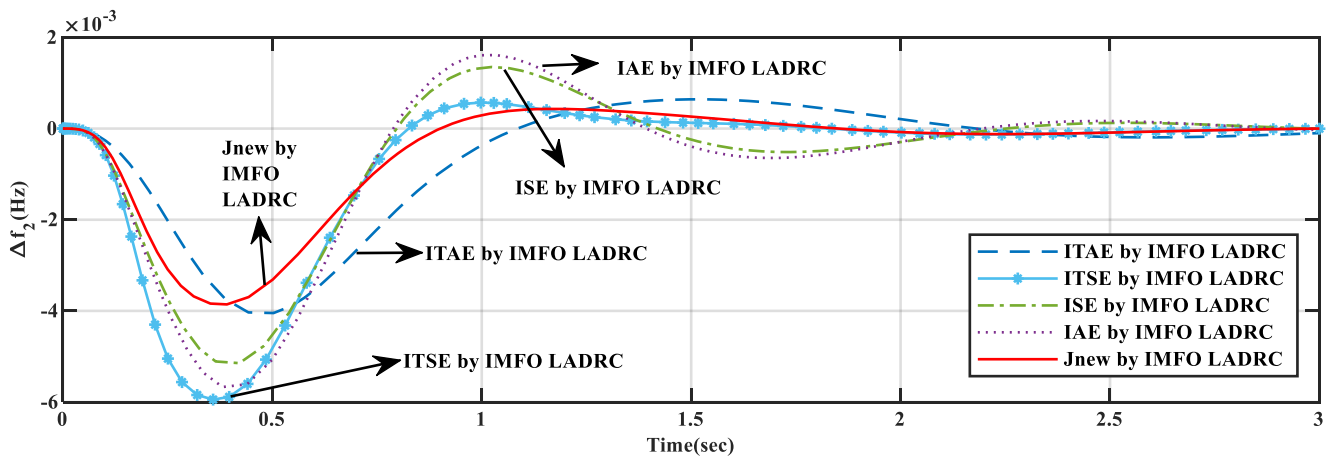


Fig.8. Change in f_2 under different objective

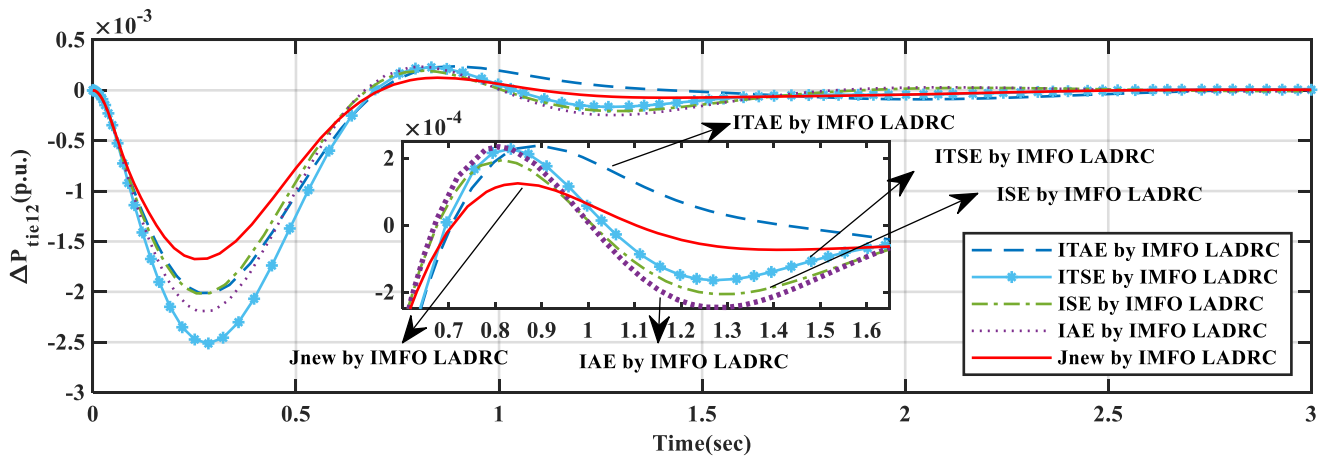


Fig.9. Change in P_{tie} under different objective

Case A: Compare with different controller types

To further demonstrate the superiority of dynamic performance from the proposed strategy, the system was tested under various step load perturbation conditions in three cases. The results are compared with the traditional PI controller, which is optimized through DE [14] and hBFOA-PSO [16], the FPI controller optimized by hPSO-PS [11] and the FPID controller optimized by IACO [12]. The evaluation indicators consist of dynamic metrics T_s , US , OS and performance index ITAE, which are calculated dynamically from system frequency response, and the

detailed data are listed in TABLE III. From the results, conventional controllers show normal control performance in more complex interconnected systems. Intelligent control methods allow for fast feedback compensation, and the calming effect of LADRC is more pronounced than fuzzy control methods in the event of load demand imbalances in the system, even while accompanied by small oscillations. By comparing with the control strategies widely used in recent years, the LADRC strategy based on the IMFO algorithm proposed in this paper shows superior performance.

TABLE III
PERFORMANCE COMPARISON OF DIFFERENT CONTROL STRATEGIES

Controller type		DE PI [14]	hBFOA-PSO PI [16]	hPSO-PS FPI [11]	IACO FPID [12]	IMFO LADRC		
Case1	$T_s(s)$ (± 0.0005)	Δf_1	10.81	10.23	5.36	1.78	1.12	
		Δf_2	11.58	10.30	6.52	3.20	0.80	
		ΔP_{tie}	9.16	8.70	5.27	2.59	0.50	
	US	Δf_1	-0.2360	-0.2472	-0.0770	-0.0231	-0.0230	
		Δf_2	-0.1945	-0.2084	-0.0300	-0.0066	-0.0046	
		ΔP_{tie}	-0.0684	-0.0738	-0.0122	-0.0027	-0.0017	
	OS	Δf_1	0.0203	0.0367	0.0000	0.0001	0.0062	
		Δf_2	0.0082	0.0276	0.0000	0.0000	0.0009	
		ΔP_{tie}	0.0011	0.0034	0.0000	0.0000	0.0000	
	ITAE	1.2551	1.1845	0.2043	0.0257	0.0036		
	Case2	$T_s(s)$ (± 0.0005)	Δf_1	12.63	11.44	8.03	3.74	1.35
			Δf_2	12.67	11.34	6.89	1.74	1.51
ΔP_{tie}			10.32	9.77	6.77	3.15	0.57	
US		Δf_1	-0.3891	-0.4169	-0.0724	-0.0218	-0.0098	
		Δf_2	-0.4720	-0.4943	-0.1721	-0.0642	-0.0477	
		ΔP_{tie}	-0.0023	-0.0069	0.0000	0.0000	0.0000	
OS		Δf_1	0.0163	0.0552	0.0000	0.0000	0.0008	
		Δf_2	0.0405	0.0735	0.0000	0.0002	0.0144	
		ΔP_{tie}	0.1368	0.1477	0.0290	0.0087	0.0036	
ITAE		2.5102	2.3691	0.6101	0.0618	0.0065		
Case3		$T_s(s)$ (± 0.0005)	Δf_1	11.67	10.33	8.30	3.68	3.05
			Δf_2	10.86	9.60	7.78	2.99	2.75
	ΔP_{tie}		9.16	8.70	6.23	2.71	2.51	
	US	Δf_1	-0.4843	-0.5226	-0.1035	-0.0292	-0.0702	
		Δf_2	-0.5455	-0.5775	-0.1780	-0.0653	-0.0389	
		ΔP_{tie}	-0.0011	-0.0034	0.0000	0.0000	-0.0108	
	OS	Δf_1	0.0017	0.0561	0.0000	0.0000	0.0185	
		Δf_2	0.0025	0.0672	0.0000	0.0000	0.0000	
		ΔP_{tie}	0.0684	0.0738	0.0176	0.0060	0.0003	
	ITAE	2.6246	2.6388	0.7407	0.0730	0.0547		

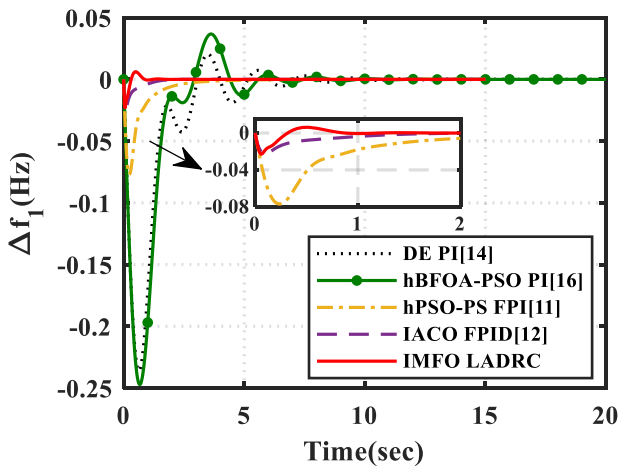


Fig.10. Change in f_1 for Case1 with different control types

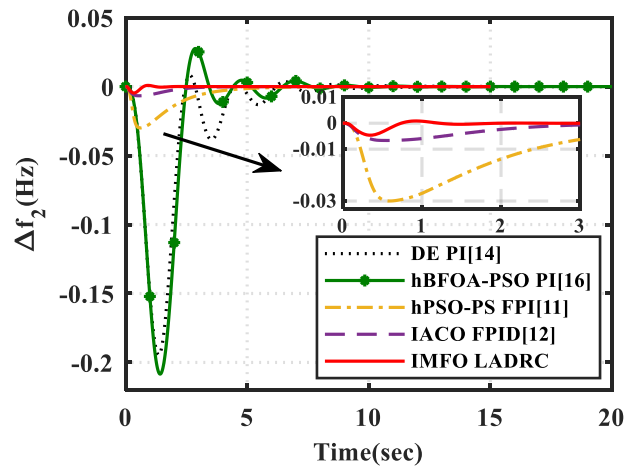


Fig.11. Change in f_2 for Case1 with different control types

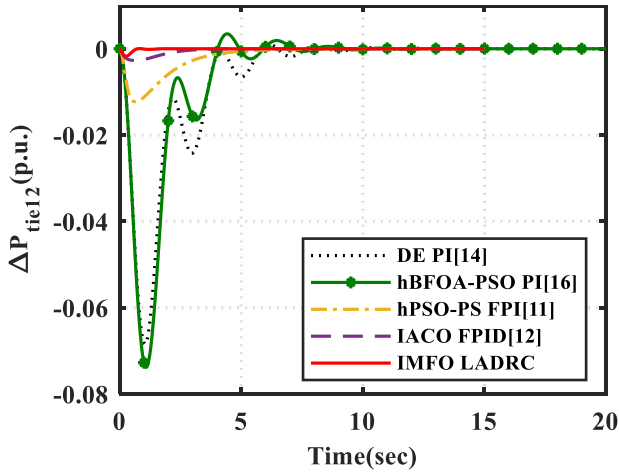


Fig.12. Change in P_{tie} for Case1 with different control types

Case1: 10% step load change rise in area1

The 10% load demand change occurs in area 1 at $t=0s$, the response curves for the LADRC based on IMFO algorithm and other comparative algorithms are shown in Fig.10-12. Regardless of through those control strategies, the system frequency can be calmed relatively quickly and the proposed strategy has excellent performance in terms of performance indicators. The objective function value of proposed control strategy ($ITAE = 0.0036$) is reduced by two orders of magnitude compared to conventional proportional-integral controllers ($ITAE = 0.7106$ [14], $ITAE = 0.7294$ [16]) and by one order of magnitude compared to the FPID controller ($ITAE = 0.0273$ [12]). Better objection metrics lead to better dynamic performance, the smallest settling time and the lowest amount of peak undershoot are obtained by proposed controller.

Case2: 20% step load change rise in area2

When the 20% load disturbance occurs in area 2, regional frequency deviation decreases as the total load demand is greater than the total generating capacity, with negative frequency deviations in Fig.13-14 and positive frequency deviations in Fig.15. The IMFO-based LADRC control strategy is significantly superior to other control strategies, allowing the system frequency to be quickly brought back to nominal values with the lowest setting time (1.35s, 1.51s, 0.57s of Δf_1 , Δf_2 , ΔP_{tie}) and reducing ITAE to 0.0065. It demonstrates that the LADRC system has the advantage of good dynamic performance in complex control strategy and guarantees the speed of regulation as well.

Case3: Step load change rise in both area

Finally, the case of each area subject to simultaneous load perturbations is also considered. The tie-line frequency deviation is positive due to the greater load variation in area 2. In Fig.16 and Fig.18, even though the proposed control strategy causes a larger overshoot phenomenon compared to the FPID control strategy based on IACO, there is a minimum regulation time (3.05s, 2.75s, 2.51s of Δf_1 , Δf_2 , ΔP_{tie}) and $ITAE = 0.0547$, for an overall optimal control performance of the proposed strategy.

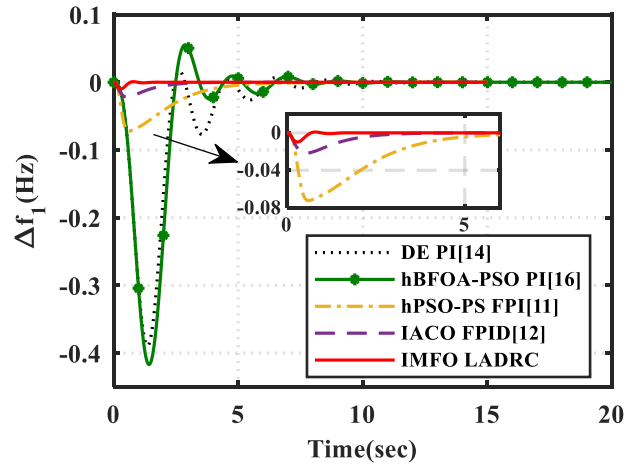


Fig.13. Change in f_1 for Case2 with different control types

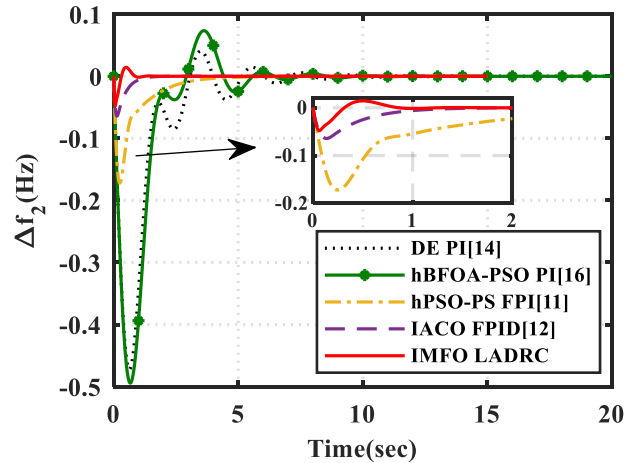


Fig.14. Change in f_2 for Case2 with different control types

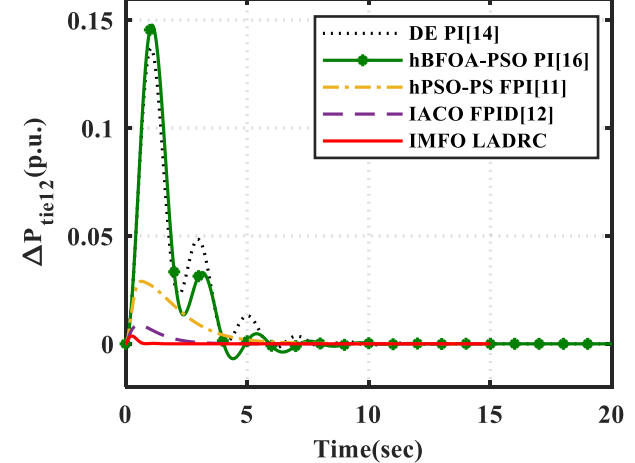


Fig.15. Change in P_{tie} for Case2 with different control types

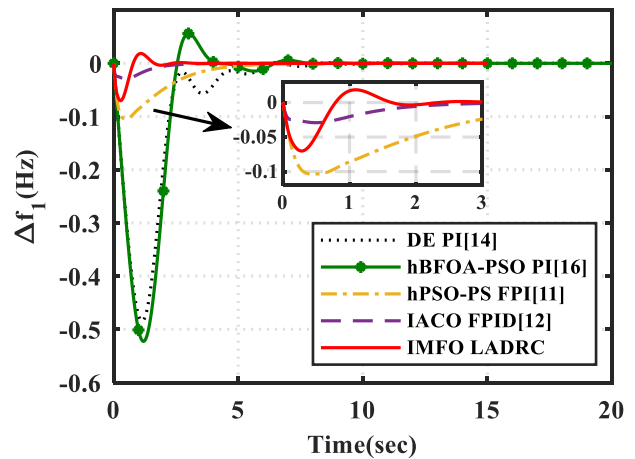


Fig.16. Change in f_1 for Case3 with different control types

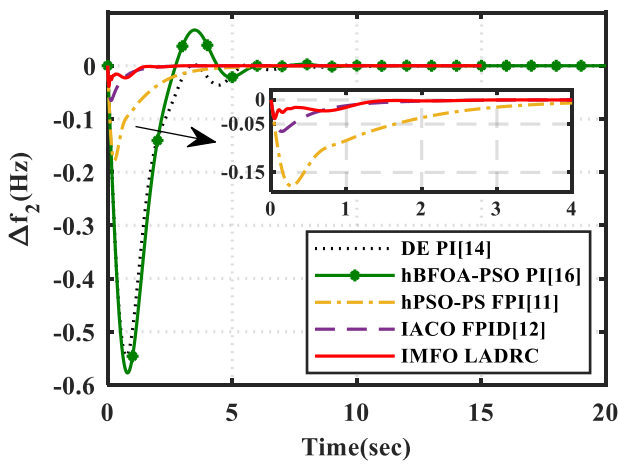


Fig.17. Change in f_2 for Case3 with different control types

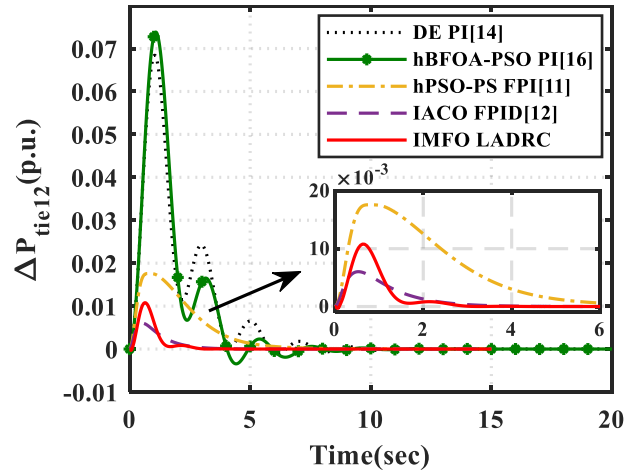


Fig.18. Change in P_{tie} for Case3 with different control type

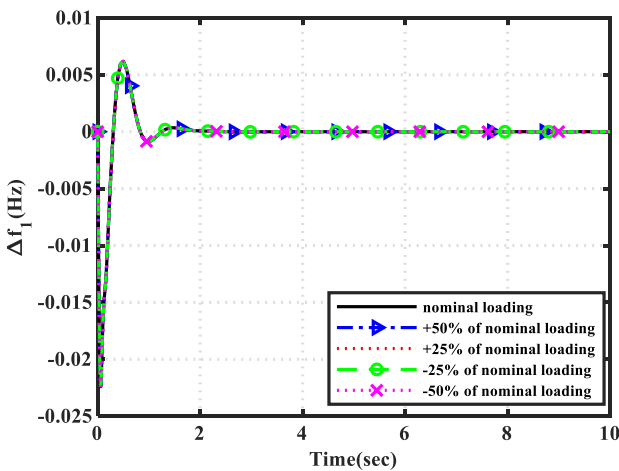


Fig.19. Change in f_1 for 10% step in area 1 with change in loading condition.

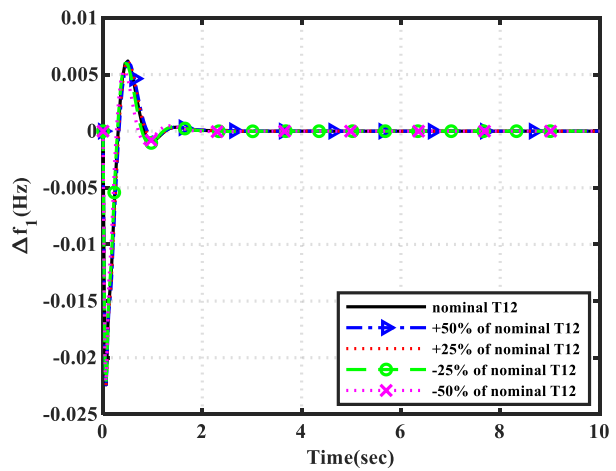


Fig.20. Change in f_1 for 10% step in area 1 with change in T_{12} .

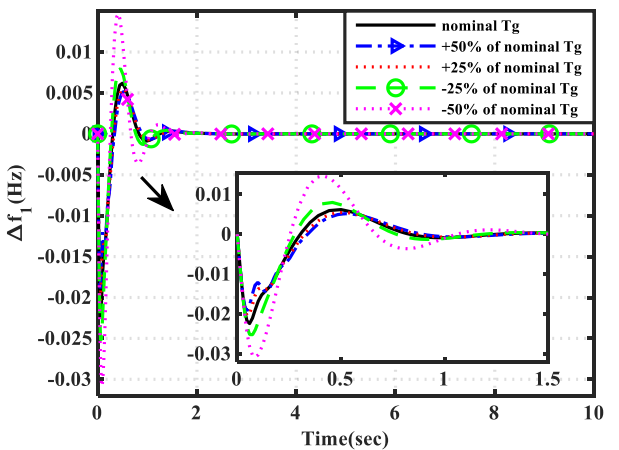


Fig.21. Change in f_1 for 10% step in area 1 with change in T_g .

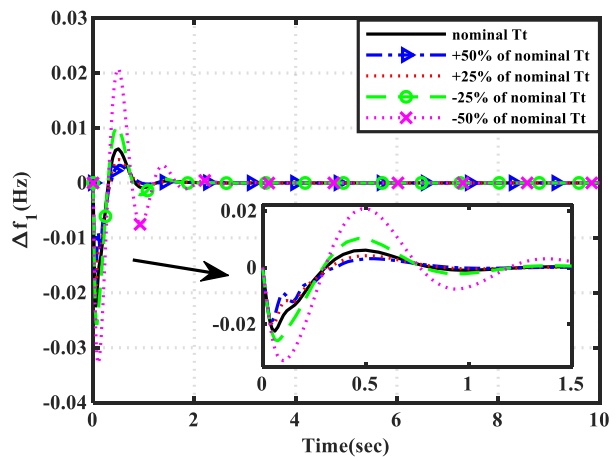


Fig.22. Change in f_1 for 10% step in area 1 with change in T_i .

Case B: Sensitivity analysis

Sensitivity analysis is gone to check the robustness of the system under changes in operating conditions and system parameters [30], the main parameters nominal loading condition and nominal T_g , T_i , T_{12} in steps of 25% in the range -50% to 50% with a SLP = 10% in area1 at $t = 0$ s. The system response curves for different test conditions are listed in Fig.19-22, the performance indicators ITAE, ITSE, ISE, IAE and the settling time T_s are indicated in TABLE IV.

As is illustrated in figures and table, the responses about the system are almost constant for changes in parameters of loading condition and T_{12} , and the response of the frequency will fluctuate with changes in T_g and T_i . Regardless of the parameter changes, the response of the system still shows small oscillations in terms of larger performance index values and longer settling time, however, as a whole the system remains well regulated and can be brought back to nominal values relatively quickly in reasonable fluctuation.

TABLE IV
SENSITIVITY ANALYSIS FOR TWO-AREA NON-REHEAT THERMAL SYSTEM

parameter variation	% change	ITAE	ITSE	ISE	IAE	settling time T_s (s)		
						Δf_1	Δf_2	ΔP_{tie}
nominal	0	0.0036	1.24E-05	6.81E-05	0.0086	1.12	0.80	0.50
loading condition	50	0.0036	1.24E-05	6.80E-05	0.0086	1.09	0.80	0.50
	25	0.0036	1.24E-05	6.80E-05	0.0086	1.12	0.80	0.50
	-25	0.0036	1.24E-05	6.81E-05	0.0086	1.12	0.80	0.50
	-50	0.0036	1.24E-05	6.82E-05	0.0086	1.09	0.80	0.50
T_g	50	0.0036	1.07E-05	5.33E-05	0.0081	1.15	0.82	0.56
	25	0.0036	1.12E-05	5.84E-05	0.0083	1.10	0.82	0.56
	-25	0.0038	1.62E-05	9.03E-05	0.0095	1.08	0.73	0.52
	-50	5.09E-03	3.49E-05	1.66E-04	0.0128	1.36	0.92	0.44
T_t	50	0.0028	6.47E-06	3.82E-05	0.0066	0.84	0.89	0.57
	25	0.0031	8.24E-06	4.82E-05	0.0073	0.82	0.84	0.55
	-25	0.0050	2.51E-05	1.16E-04	0.01163	1.50	1.27	0.52
	-50	0.0114	9.16E-05	2.89E-04	0.0208	1.97	1.24	0.93
T_{12}	50	0.0036	1.26E-05	7.00E-05	0.0084	1.07	0.90	0.56
	25	0.0035	1.26E-05	6.93E-05	0.0085	1.11	0.85	0.56
	-25	0.0037	1.20E-05	6.59E-05	0.0088	1.10	1.28	0.50
	-50	0.0036	1.08E-05	6.17E-05	0.0087	0.99	1.24	0.80

B. Extension to non-linear power system

For testing the effectiveness of the proposed control strategy in a non-linear system, the governor dead band (GDB) is considered as a non-linear factor to be introduced into the study system built in Fig.23. The GDB is referred to a situation where the speed changes continuously within a certain range but the valve opening of the valve position does not change. At the moment of a power system existing with a GDB phenomenon, the system frequency will deviate from the nominal value and accompanied with continuous oscillations, so the control effect of the controller under non-linear factors is of great importance in practical operation. In the study, GDB was expressed linearly by describing function approach and Fourier expansion, the expression for governor was defined as [31]:

$$G_g(s) = \frac{0.8 - \frac{0.2}{\pi}}{1 + T_g s} \quad (24)$$

The transfer function model of the system with the inclusion of the governor dead band is given in Fig.23. Nominal system parameters are illustrated in Appendix B.

In the study of a two-area power system with GDB, the 1% perturbation is placed in area 1 at $t = 0$ s. The influence of ISE and the modified objective function J_5 is considered. The LADRC parameters optimized through the ISE objective function are $w_{c1} = 4.8814$, $b_1 = 64.2956$, $w_{c2} = 1.4066$, $b_2 = 82.9994$, and the LADRC parameters optimized through J_5 are $w_{c1} = 5$, $b_1 = 54.4457$, $w_{c2} = 2.4889$, $b_2 =$

68.7089. hBFOA-PSO [16] and CRAZY_PSO [31] optimized PI controllers are utilized for comparison. The frequency response curves of the system (Δf_1 , Δf_2 and ΔP_{tie}) under the same experimental conditions are shown in Fig.24-26, the objection indicator ISE and dynamic performance of those are presented in the TABLE V. As can be seen from the table, the fastest regulation speed of $T_s = 0.80(s)$ can be achieved via the IMFO optimized LADRC through J_5 . Comparing the optimal solutions of all the cited literature, the minimum of ISE = 3.50E-05 is obtained by this paper relative to hBFOA-PSO optimized PI (ISE = 2.10E-04) and CRAZY_PSO optimized PI (ISE = 2.20E-04). Reflected in Fig.24-26, in circumstances of the system with unbalanced load demand, the frequency response under PI controller optimized through ISE objective function is subject to a continuous disturbance, while LADRC can calm the system faster. In addition, the parameter searching of LADRC through J_5 can obtain smaller oscillation phenomena. As a result, there is significant improvement in the control performance of the proposed strategy in nonlinear systems with GDB.

To further confirm the stability of the proposed strategy, the stochastic step load change shown in Fig.27 is placed in area 1 of the system. As can be seen from the frequency deviation response curves shown in Fig.28, in the face of more rigorous load conditions, the proposed strategy can compensate system imbalance and shows superior transient response.

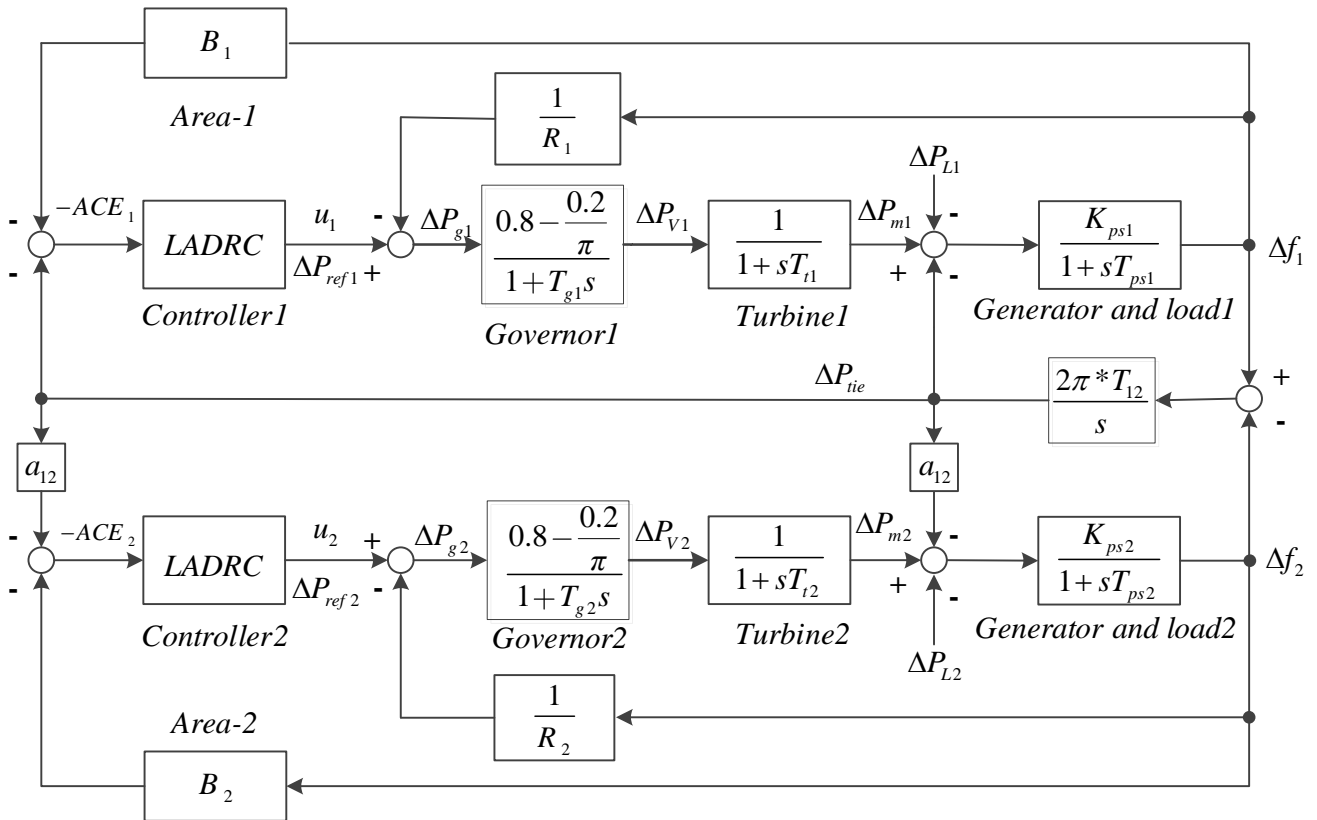


Fig.23. Transfer function model of two-area power system with GDB

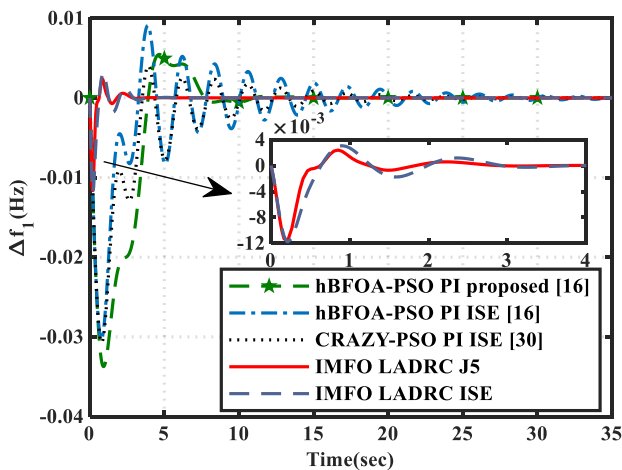


Fig.24. Change in f_1 for 1% step increase in area 1

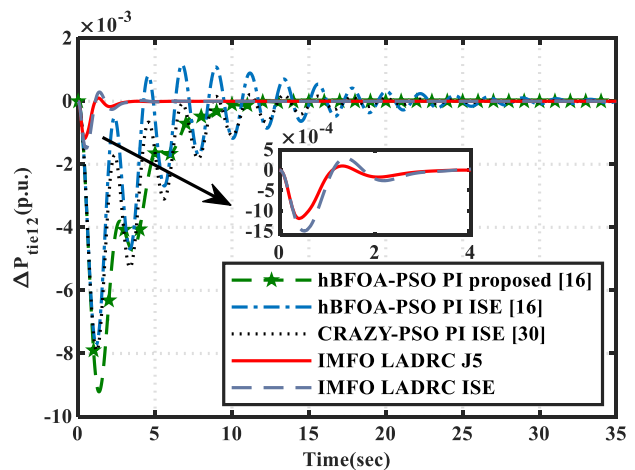


Fig.25. Change in P_{tie} for 1% step increase in area 1

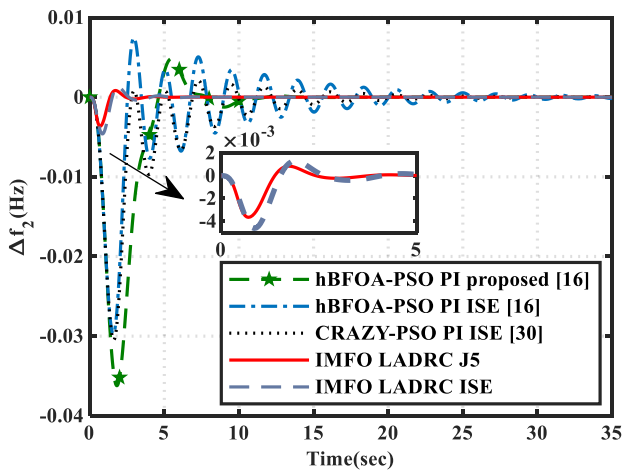


Fig.26. Change in f_2 for 1% step increase in area 1

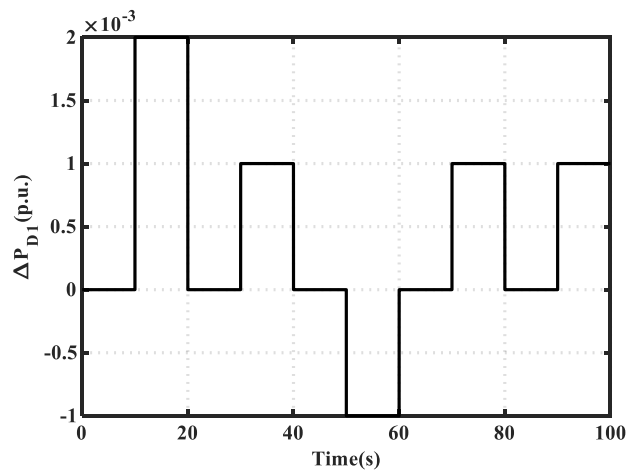


Fig.27. Random step load disturbance

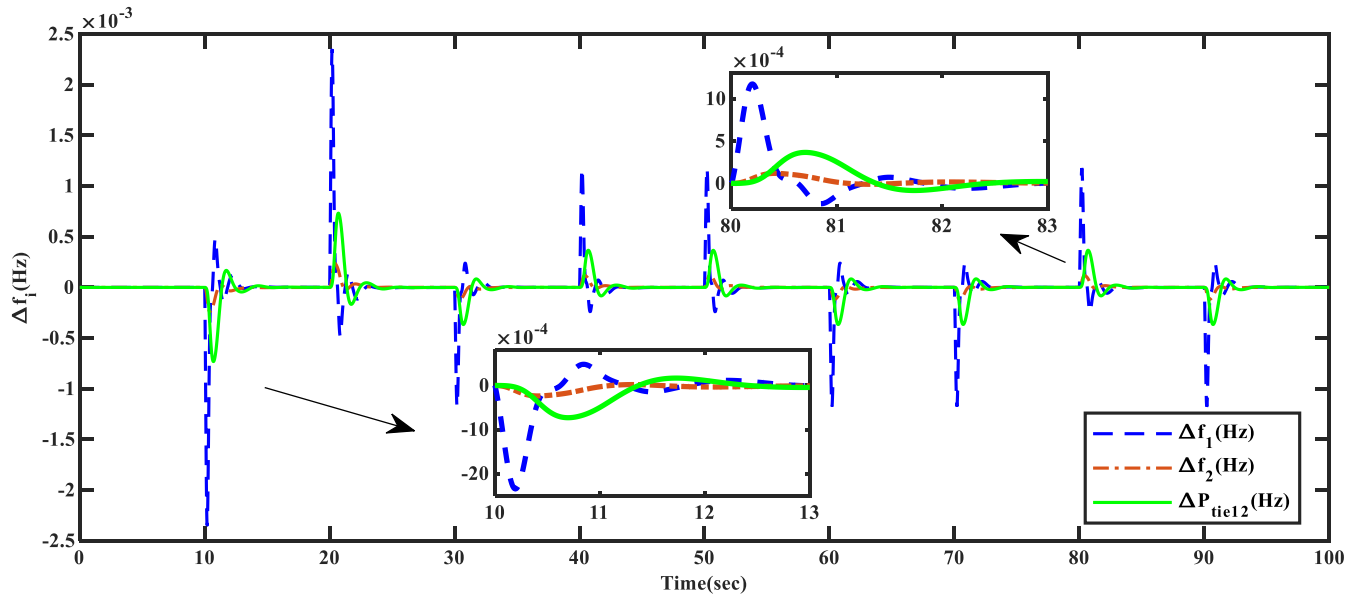


Fig.28. Change in f_i for 1% Random step load disturbance in area 1

TABLE V
PERFORMANCE COMPARISON OF DIFFERENT CONTROL STRATEGIES

Controller type	hBFOA-PSO PI [16] (ISE objective function)	hBFOA-PSO PI [16] (proposed objective function)	CRAZY_PSO PI [31] (ISE objective function)	IMFO LADRC (ISE objective function)	IMFO LADRC (modified objective function J_5)
T_s	Δf_1	24.48	10.19	19.59	2.72
	Δf_2	24.48	9.99	19.61	2.31
	ΔP_{tie}	15.71	8.30	12.54	0.90
US	Δf_1	-0.0303	-0.0337	-0.0307	-0.0118
	Δf_2	-0.0297	-0.0362	-0.0305	-0.0046
	ΔP_{tie}	-0.0077	-0.0092	-0.0079	-0.0015
OS	Δf_1	0.0091	0.0055	0.0040	0.0031
	Δf_2	0.0075	0.0048	0.0021	0.0013
	ΔP_{tie}	0.0012	3.21E-06	0.0002	0.0003
ISE	2.10E-04	3.80E-04	2.20E-04	5.28E-05	3.50E-05

TABLE VI
PERFORMANCE COMPARISON OF DIFFERENT CONTROL STRATEGIES

Controller type	MFO PI[23]	MFO PID[23]	GWO PID[17]	IMFO LADRC
T_s	Δf_1	19.64	13.49	8.98
	Δf_2	12.49	9.91	10.72
	Δf_3	16.58	11.54	10.46
US	Δf_1	-0.0426	-0.0364	-0.0260
	Δf_2	-0.0280	-0.0206	-0.0102
	Δf_3	-0.0288	-0.0221	-0.0117
OS	Δf_1	0.0231	0.0217	0.0035
	Δf_2	0.0107	0.0076	8.80E-05
	Δf_3	0.0148	0.0109	9.51E-05
ITAE	1.7123	0.8381	0.6960	0.0073
ITSE	0.0133	0.0051	0.0020	5.58E-06
ISE	0.0054	0.0028	0.0010	1.63E-05
IAE	0.3868	0.2416	0.1775	0.0068

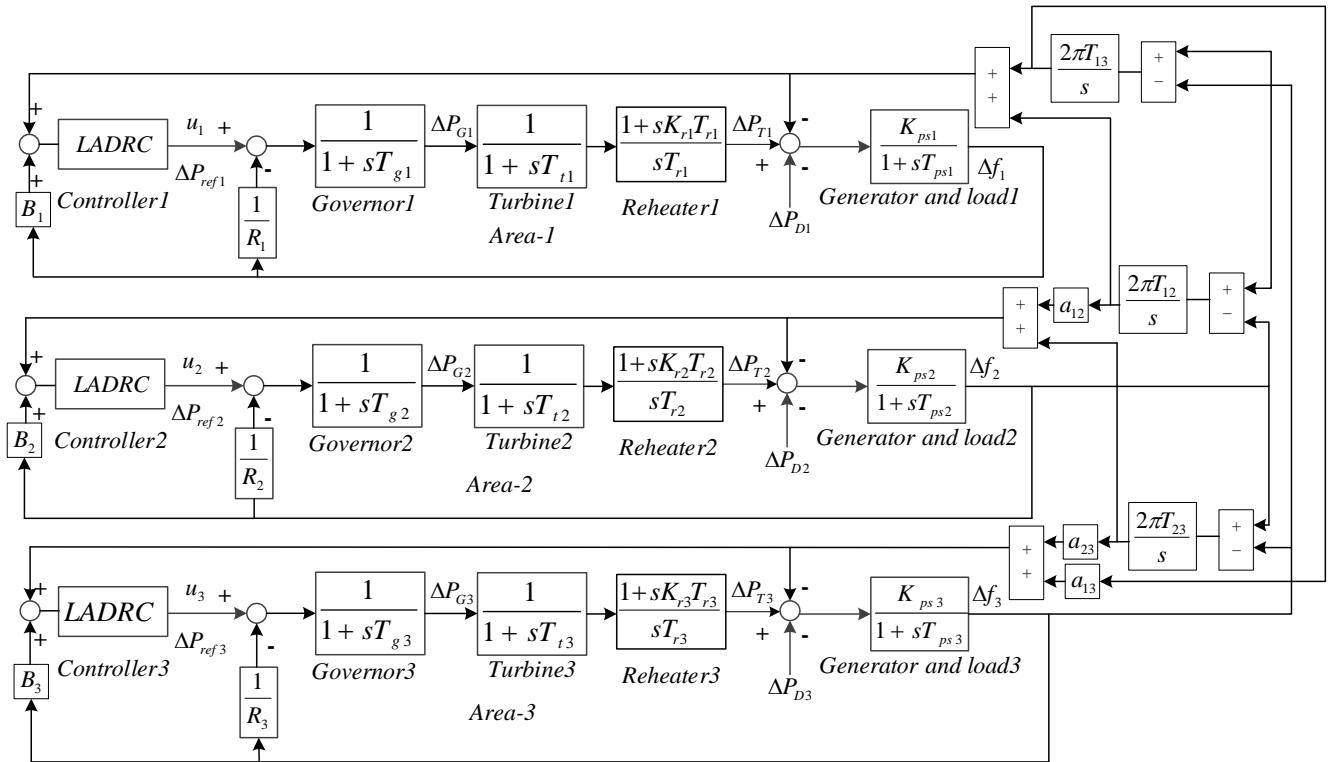


Fig.29. Transfer function model of three-area reheat thermal power system

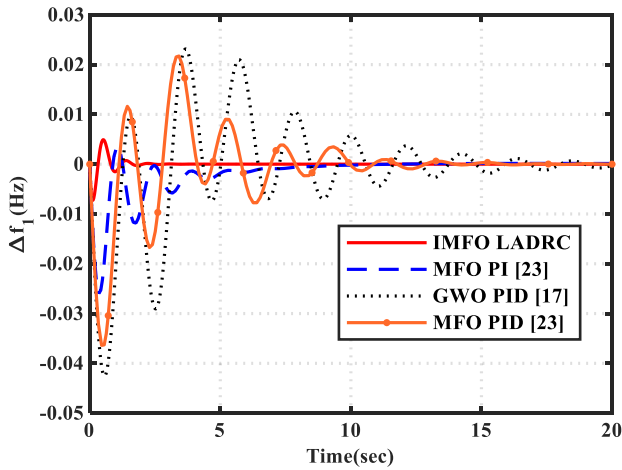


Fig.30. Change in f_1 for 2% step increase in area 1

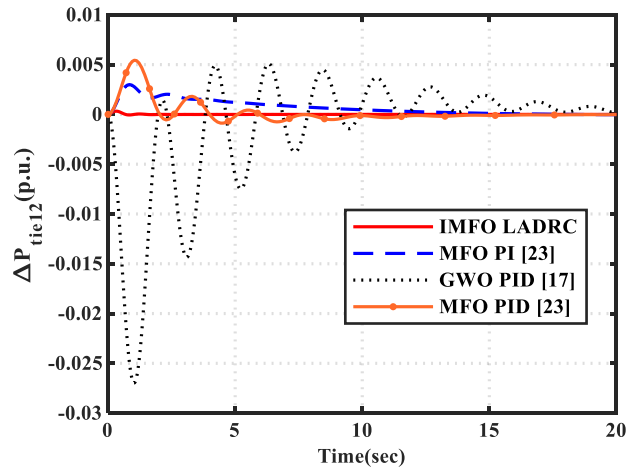


Fig.31. Change in P_{tie12} for 2% step increase in area 1

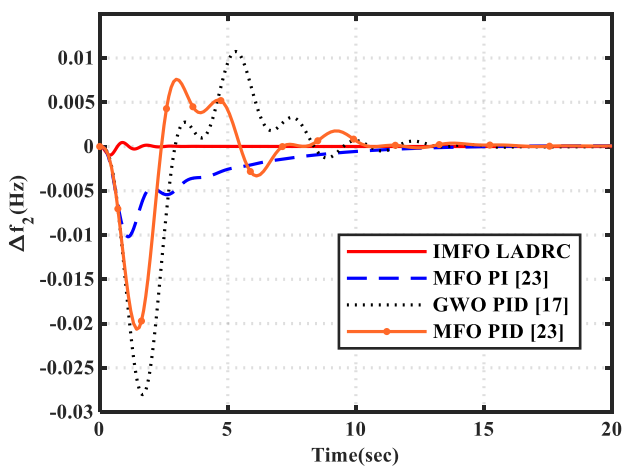


Fig.32. Change in f_2 for 2% step increase in area 1

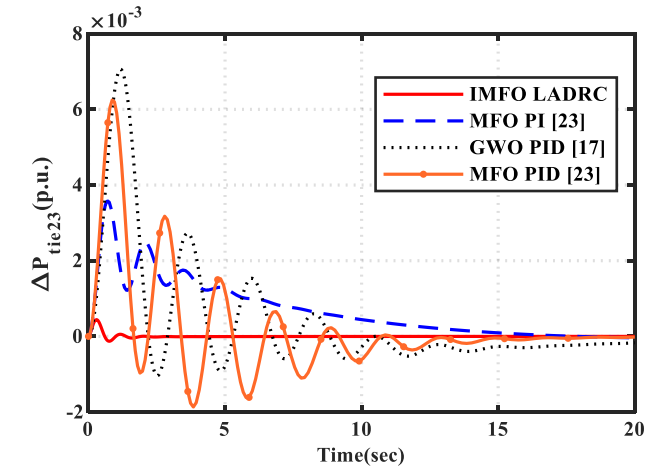


Fig.33. Change in P_{tie23} for 2% step increase in area 1

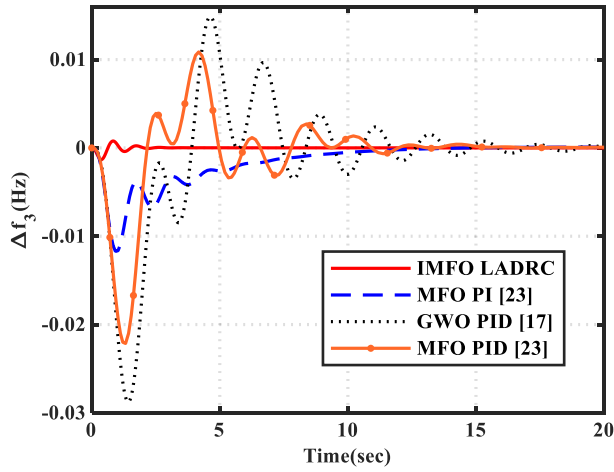


Fig.34. Change in f_3 for 2% step increase in area 1

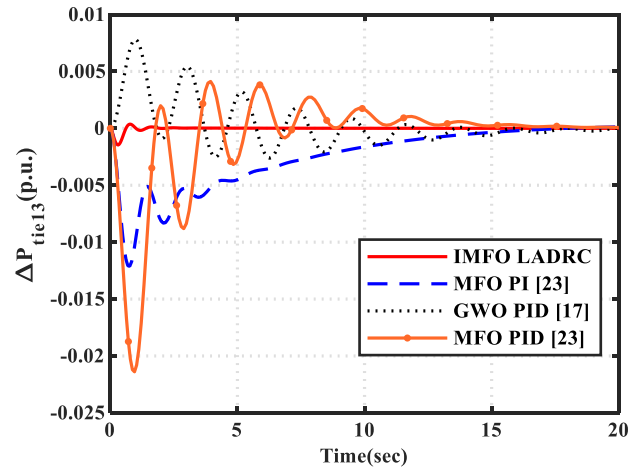


Fig.35. Change in P_{tie13} for 2% step increase in area 1

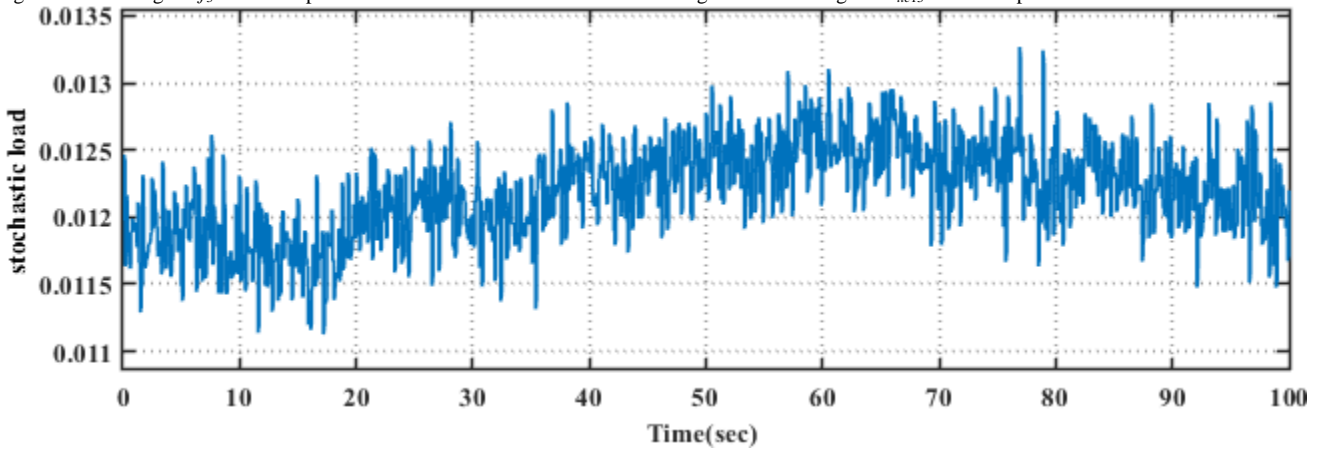


Fig.36. Stochastic load

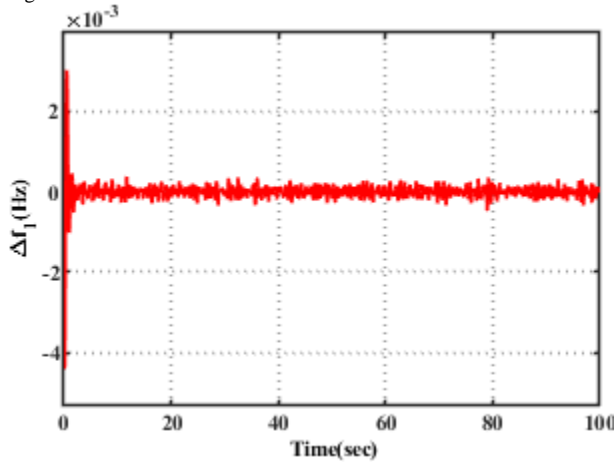


Fig.37. Change in f_1 for stochastic load increase in area 1

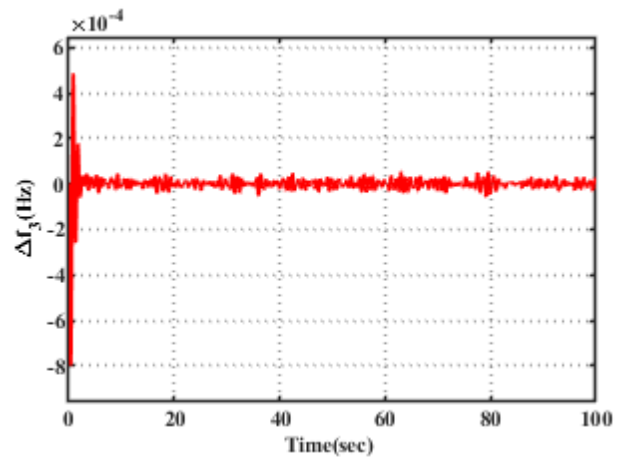


Fig.39. Change in f_3 for stochastic load increase in area 1

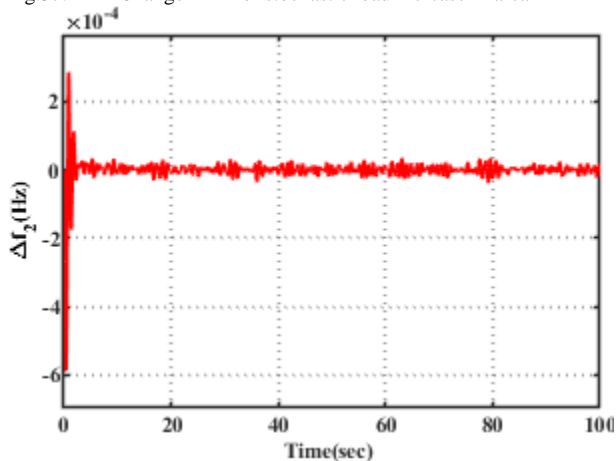


Fig.38. Change in f_2 for stochastic load increase in area 1

C. Extension to three-area reheat thermal power system

To demonstrate the capabilities of the proposed control strategy in a multi-area power interconnection system, an unequal three-area reheat thermal power system constructed in Fig.29 is employed [32]. The system consists of three interconnected reheat thermal plants, the control power rating of area1/2/3 is 2000 MW, 5000 MW and 8000 MW. Nominal values of system parameters are illustrated in Appendix C. The LADRC controllers with equivalent parameters are configured in each area, the modified objective function is used to optimize the controller parameters to $w_c = 10$ and $b = 97.59701$ via the IMFO algorithm. MFO optimized PID controller and GWO optimized PID controller are used to compare in three-area reheat thermal power system. A SLP = 2% is given in area 1

at $t = 0$ s, the responses curves of the system frequency deviations (Δf_1 , Δf_2 and Δf_3) and the incremental changes in tie-line power (ΔP_{tie12} , ΔP_{tie13} and ΔP_{tie23}) are shown in Fig.30-35. And the analytical indicators of the system frequency deviations are given in TABLE VI, including calculated value of performance indicator functions ITAE, ITSE, ISE, IAE and dynamic indicators settling time T_s , peak undershoot US and peak overshoot OS . As can be seen from Fig.30-35 and TABLE VI, the LADRC has excellent control effect during the secondary regulation of the LFC when a sudden load demand imbalance occurs in three-area unequal reheat thermal power system, which can bring the system frequency back to its nominal value quickly. In the results of simulations that compared with the PI, PID controllers based on MFO algorithm and PID controller based on GWO algorithm, it is apparent that the IMFO optimized LADRC controller can obtain broken values in terms of lowest T_s and minimum overshoot, with the performance index function values of ITAE = 0.0073, ITSE = 5.58E-06, ISE = 1.63E-05, IAE = 0.0068. In order to simulate the load conditions in practice, a stochastic load is set in area 1 of the system as shown in the Fig.36 and the frequency response of each area is shown in the Fig.37-39. From the graphs it can be observed that the LADRC controller regulated by the IMFO algorithm reduces the amplitude of the oscillations and the regulation time of the system. It can be concluded that the proposed control strategy has strong applicability in more complex multi-area interconnected power systems.

V. CONCLUSION

This paper focuses on the optimization of AGC problems and a LADRC control strategy based on the IMFO algorithm is proposed. The LADRC controller is designed for the structural characteristics of the interconnected power system and its parameters are selected by using the improved MFO algorithm through a new objective function proposed. Firstly, the control strategy is simulated in detail in a two-area non-reheat thermal system, comparing it with the MFO algorithm and conventional PID controller. The simulation results demonstrate that the IMFO optimized control performance of the LADRC controller is significantly improved. Secondly, in comparison to the four widely used objective functions, the proposed objective function can obtain smoother oscillations and faster regulation time in the optimization of controller parameters. To further demonstrate the superiority of the LADRC controller based on the IMFO algorithm, the result of ITAE = 0.0036 is superior to the DE and hBFOA-PSO optimized PI controller, hPSO-PS optimized FPI controller, IACO optimized FPID controller in recent literatures and has been verified in sensitivity analysis for robustness. To test the potential of the proposed control strategy, its application is extended to nonlinear and unequal systems. In the two-area power system with GDB, the proposed method can achieve the smallest value of the objective function (ISE = 3.50E-05) related to the hBFOA-PSO optimized PI and CRAZY_PSO optimized PI. And the results of the proposed control strategy (ITAE = 0.0073, ITSE = 5.58E-06, ISE = 1.63E-05, IAE = 0.0068) are superior to those of the MFO optimized PI, PID controllers and the GWO optimized PID controller

in three-area reheat thermal power system, so the higher control performance is clearly proven.

APPENDIX

Appendix A: nominal parameters of two-area non-reheat power system [11, 12, 14, 16]

$P_{r1} = P_{r2} = 2000$ MW; $f = 60$ Hz; $P_{L1} = P_{L2} = 1000$ MW; $T_{i1} = T_{i2} = 0.3$ s; $T_{g1} = T_{g2} = 0.08$ s; $B_1 = B_2 = 0.425$ p.u.MW/Hz; $R_1 = R_2 = 2.4$ Hz/p.u.; $K_{ps1} = K_{ps2} = 120$ Hz/p.u.MW; $T_{ps1} = T_{ps2} = 20$ s; $T_{12} = 0.545$ p.u.; $a_{12} = -P_{r1}/P_{r2} = -1$.

Appendix B: nominal parameters of two-area power system with GDB [16, 30]

$B_1 = B_2 = 0.425$ p.u.MW/Hz; $R_1 = R_2 = 2.0$ Hz/p.u.; $T_{g1} = T_{g2} = 0.2$ s; $T_{i1} = T_{i2} = 0.3$ s; $K_{ps1} = K_{ps2} = 120$ Hz/p.u.MW; $T_{ps1} = T_{ps2} = 20$ s; $T_{12} = 0.0707$ p.u.; $a_{12} = -1$.

Appendix C: nominal parameters of unequal three-area reheat thermal power system [32]

$P_{r1} = 2000$ MW; $P_{r2} = 5000$ MW; $P_{r3} = 8000$ MW; $B_1 = B_2 = B_3 = 0.425$ p.u.MW/Hz; $R_1 = R_2 = R_3 = 2.0$ Hz/p.u.; $T_{g1} = T_{g2} = T_{g3} = 0.08$ s; $T_{i1} = T_{i2} = T_{i3} = 0.3$ s; $T_{r1} = T_{r2} = T_{r3} = 10$ s; $T_{ps1} = T_{ps2} = T_{ps3} = 20$ s; $K_{r1} = K_{r2} = K_{r3} = 0.5$; $K_{ps1} = K_{ps2} = K_{ps3} = 120$ Hz/p.u.; $T_{12} = T_{13} = T_{23} = 0.545$ p.u.; $R_1 = R_2 = R_3 = 2.4$ Hz/p.u.; $a_{12} = -2/5$; $a_{13} = -5/8$; $a_{23} = -2/8$; $D_1 = D_2 = D_3 = 0.00833$ p.u.MW/Hz.

REFERENCES

- [1] K. Ullah, A. Basit, Z. Ullah, S. Aslam and H. Herodotou, "Automatic generation control strategies in conventional and modern power systems: A comprehensive overview," *Energies*, vol. 14, no. 9, pp. 2376-2418, 2021.
- [2] R. Shankar, S. R. Pradhan, K. Chatterjee and R. Mandal, "A comprehensive state of the art literature survey on LFC mechanism for power system," *Renewable and Sustainable Energy Reviews*, vol. 76, pp. 1185-1207, 2017.
- [3] H. Shayeghi, H. A. Shayanfar and A. Jalili, "Load frequency control strategies: A state-of-the-art survey for the researcher," *Energy Conversion and Management*, vol. 50, no. 2, pp. 344-353, 2009.
- [4] K. Chatterjee, "Design of dual mode PI controller for load frequency control," *International Journal of Emerging Electric Power Systems*, vol. 11, no. 4, 2010.
- [5] Y. Arya and N. Kumar, "Optimal control strategy-based AGC of electrical power systems: A comparative performance analysis," *Optimal Control Applications and Methods*, vol. 38, no. 6, pp. 982-992, 2017.
- [6] M. H. Kazemi, M. Karrari and M. B. Menhaj, "Decentralized robust adaptive-output feedback controller for power system load frequency control," *Electrical Engineering*, vol. 84, no. 2, pp. 75-83, 2002.
- [7] S. Sahoo, N. K. Jena, G. Dei and B. K. Sahu, "Self-adaptive fuzzy-PID controller for AGC study in deregulated power system," *Indonesian Journal of Electrical Engineering and Informatics*, vol. 7, no. 4, pp. 650-663, 2020.
- [8] B. Mohanty, "TLBO optimized sliding mode controller for multi-area multi-source nonlinear interconnected AGC system," *International Journal of Electrical Power & Energy Systems*, vol. 73, pp. 872-881, 2015.
- [9] Z. Al-Hamouz, H. Al-Duwaish and N. Al-Musabi, "Optimal design of a sliding mode AGC controller: Application to a nonlinear interconnected model," *Electric Power Systems Research*, vol. 81, no. 7, pp. 1403-1409, 2011.
- [10] P. Mc Namara and F. Milano, "Efficient implementation of MPC-based AGC for real-world systems with low inertia," *Electric Power Systems Research*, vol. 158, pp. 315-323, 2018.
- [11] R. K. Sahu, S. Panda and G. T. Chandra Sekhar, "A novel hybrid PSO-PS optimized fuzzy PI controller for AGC in multi area interconnected power systems," *International Journal of Electrical Power & Energy Systems*, vol. 64, pp. 880-893, 2015.
- [12] G. Chen, Z. Li, Z. Zhang and S. Li, "An Improved ACO algorithm optimized fuzzy PID controller for load frequency control in multi area interconnected power systems," *IEEE Access*, vol. 8, pp. 6429-

- 6447, 2020.
- [13] F. Daneshfar and H. Bevrani, "Multi objective design of load frequency control using genetic algorithms," *International Journal of Electrical Power & Energy Systems*, vol. 42, no. 1, pp. 257-263, 2012.
- [14] U. K. Rout, R. K. Sahu and S. Panda, "Design and analysis of differential evolution algorithm based automatic generation control for interconnected power system," *Ain Shams Engineering Journal*, vol. 4, no. 3, pp. 409-421, 2013.
- [15] E. S. Ali and S. M. Abd-Elazim, "Bacteria foraging optimization algorithm based load frequency controller for interconnected power system," *International Journal of Electrical Power & Energy Systems*, vol. 33, no. 3, pp. 633-638, 2011.
- [16] S. Panda, B. Mohanty and P. K. Hota, "Hybrid BFOA-PSO algorithm for automatic generation control of linear and nonlinear interconnected power systems," *Applied Soft Computing*, vol. 13, no. 12, pp. 4718-4730, 2013.
- [17] R. K. Mallick, F. Haque, R. R. Rout and M. K. Debnath, "Application of grey wolves-based optimization technique in multi-area automatic generation control," *2016 International Conference on Electrical, Electronics, and Optimization Techniques*, pp. 269-274.
- [18] J. Han, "From PID to active disturbance rejection control," *IEEE Transactions on Industrial Electronics*, vol. 56, no. 3, pp. 900-906, 2009.
- [19] C. Zengqiang, H. Zhaoyang and S. Mingwei, "Active disturbance rejection control of load frequency based on big probability variation's genetic algorithm for parameter optimization," *CAAI transactions on intelligent systems*, vol. 15, no. 01, pp. 41-49, 2020.
- [20] K. Liu, J. He, Z. Luo and H. Shan, et al., "Load frequency control of pumped storage power station based on LADRC," *Processes*, vol. 8, no. 4, pp. 380, 2020.
- [21] Y. Zheng, Z. Chen, Z. Huang, M. Sun and Q. Sun, "Active disturbance rejection controller for multi-area interconnected power system based on reinforcement learning," *Neurocomputing*, vol. 425, pp. 149-159, 2021.
- [22] W. Tan, Y. Hao and D. Li, "Load frequency control in deregulated environments via active disturbance rejection," *International Journal of Electrical Power & Energy Systems*, vol. 66, pp. 166-177, 2015.
- [23] D. K. Lal, K. K. Bhoi and A. K. Barisal, "Performance evaluation of MFO algorithm for AGC of a multi area power system," in *International Conference on Signal Processing, Communication, Power and Embedded System 2016*, pp. 903-908.
- [24] O. I. Elgerd and H. H. Happ, "Electric energy systems theory: An introduction," *IEEE Transactions on Systems, Man, and Cybernetics*, vol. SMC-2, no. 2, pp. 296-297, 1972.
- [25] Y. Lie, D. Lie, X. Qinlan and Y. Fangli, "Active disturbance rejection control of position control for electrohydraulic servo system," *Engineering Letter*, vol. 3, no. 28, pp. 944-948, 2020.
- [26] Z. Gao, "Scaling and bandwidth-parameterization based controller tuning," in *Proceedings of the 2003 American Control Conference*, pp. 4989-4996.
- [27] Y. Arya, P. Dahiya, E. Çelik, G. Sharma, H. Gozde and I. Nasiruddin, "AGC performance amelioration in multi-area interconnected thermal and thermal-hydro-gas power systems using a novel controller," *Engineering Science and Technology, an International Journal*, vol. 24, no. 2, pp. 384-396, 2021.
- [28] S. Mirjalili, "Moth-flame optimization algorithm: A novel nature-inspired heuristic paradigm," *Knowledge-Based Systems*, vol. 89, pp. 228-249, 2015.
- [29] H. Wang, H. Li, Y. Liu, C. Li and S. Zeng, "Opposition-based particle swarm algorithm with cauchy mutation," in *IEEE Congress on Evolutionary Computation 2007*, pp. 4750-4756.
- [30] R. K. Sahu, S. Panda and U. K. Rout, "DE optimized parallel 2-DOF PID controller for load frequency control of power system with governor dead-band nonlinearity," *International Journal of Electrical Power & Energy Systems*, vol. 49, pp. 19-33, 2013.
- [31] H. Gozde and M. C. Taplamacioglu, "Automatic generation control application with Craziness based particle swarm optimization in a thermal power system," *International Journal of Electrical Power & Energy Systems*, vol. 33, no. 1, pp. 8-16, 2011.
- [32] J. Nanda, S. Mishra and L. C. Saikia, "Maiden application of bacterial foraging-based optimization technique in multiarea automatic generation control," *IEEE Transactions on Power Systems*, vol. 24, no. 2, pp. 602-609, 2009.